Chemical Engineering Journal 148 (2009) 26–34

Contents lists available at ScienceDirect

Chemical Engineering Journal

journal homepage: www.elsevier.com/locate/cej

Biosorption of Reactive Blue 49 dye under batch and continuous mode using a mixed biosorbent of macro-fungus *Agaricus bisporus* and *Thuja orientalis* cones

Sibel Tunali Akar[a,*], Asli Gorgulu[b], Zerrin Kaynak[a], Burcu Anilan[b], Tamer Akar[a]

[a] Department of Chemistry, Faculty of Arts and Science, Eskişehir Osmangazi University, Campus of Meşelik, 26480 Eskişehir, Turkey
[b] Department of Chemistry Education, Faculty of Education, Eskişehir Osmangazi University, 26480 Eskişehir, Turkey

ARTICLE INFO

Article history:
Received 24 March 2008
Received in revised form 10 July 2008
Accepted 13 July 2008

Keywords:
Agaricus bisporus
Thuja orientalis
Biosorption
Dye pollution
Kinetics
Isotherm

ABSTRACT

A biosorbent was developed by mixing the macro-fungus *Agaricus bisporus* and *Thuja orientalis* cones and successfully used for the biosorption of Reactive Blue 49 (RB49) dye. The biosorbent system was evaluated in batch and continuous biosorption process. A series of batch studies was carried out to identify the optimum biosorption conditions such as pH, biosorbent dosage and equilibrium time. The biosorption process followed the pseudo-first-order and the pseudo-second-order kinetic models and the Freundlich, Langmuir and Dubinin–Radushkevich (D–R) isotherm models at different temperatures. The maximum biosorption capacity of the mixed biomass system was 1.85×10^{-4} mol g^{-1} at 45 °C. The negative ΔG° values and the positive ΔH° values indicated that the biosorption process was spontaneous and endothermic. The dynamic flow biosorption potential of the biomass system was investigated as a function of the flow rate, column size and inlet solute concentration. FTIR and SEM analysis were used to characterize the biosorbent and biosorption mechanism. The functional groups such as carboxyl, amine, amide and hydroxyl on the biosorbent surface may be responsible for RB49 biosorption. In combination, our results suggest that this eco-friendly and economical biomass system may be useful for the removal of contaminating reactive dyes.

1. Introduction

Synthetic dyes from the effluents of textile industry are known to be a major source of environmental pollution, in terms of both the volume of dye discharged and the effluent composition [1]. Approximately 1 million kilograms of dye are discharged in effluents from the textile industry each year in the world [2].

Based on dyeing processes, textile/tannery dyes may be classified as acid, basic, direct, disperse, mordant, reactive, sulfur, azoic and vat dyes. Reactive textile dyes are highly water-soluble anionic dyes. They differ from the other classes of dyes since they covalently bind to textile fibers and cannot be easily removed by conventional treatment processes due to their stability under light, heat, oxidizing agents and biological degradation [3,4]. Textile dye effluents contain reactive dyes in a concentration range of 5–1500 mg L^{-1}. Therefore, the treatment of dye-contaminated effluents is currently a primary environmental concern [5].

Biosorption technology utilizing different types of biomasses is environmentally important since they can be used to remove toxic compounds from contaminated effluents [6]. The dye biosorption potentials of many different biological materials have previously been reported upon, including *Aspergillus niger* [7], *Chlorella vulgaris* [8], *Caulerpa scalpelliformis* [9], *Phaseolus vulgaris* L. [10] and *Trametes versicolor* [11].

The advantages of macro-fungus-based biomasses such as easily and economically available anywhere, chemical stability in most alkaline and acidic conditions and good mechanical properties make them attractive in the biosorption studies. Furthermore, the fruiting bodies of the macro-fungi have a tough texture when dried and have other physical characteristics which are conductive their development into adsorbents [12,13].

The macro-fungus *Agaricus bisporus*, commonly known as a mushroom, is an edible basidomycete and is commercially available. The main components of the fungal cell wall are polysaccharides (80–90% of the dry mass). Chitin is characteristic component of the basidomycetes [14]. *A. bisporus* was chosen as a biosorbent material in this study because there is relatively little information in the literature regarding its dye biosorption capability. *Thuja orientalis* cones are economical, and are a natural biomaterial that is widely available in large quantities. The mature cones contain hemicellulose, cellulose, lignin, rosin and tannins [15]. Previous studies have reported that *T. orientalis* cones have

* Corresponding author. Tel.: +90 222 2393750/2862; fax: +90 222 2393578.
E-mail address: stunali@ogu.edu.tr (S.T. Akar).

1385-8947/$ – see front matter © 2008 Elsevier B.V. All rights reserved.
doi:10.1016/j.cej.2008.07.027

the capacity to bind metals [15–17] and dyes [18]. However, there is currently no information regarding the use of *T. orientalis* cones as biomatrix and limited information on the wastewater treatment using mixed adsorbents in the literature.

In the current study, the macro-fungus *A. bisporus* and *T. orientalis* cone biomatrix were mixed well and employed as mixed biosorbent. Its biosorption potential was analyzed using Reactive Blue 49 (RB49) as a model dye. The biosorption behavior of the mixed biosorbent was examined by the Freundlich, Langmuir, Dubinin–Radushkevich (D–R) isotherms, the pseudo-first-order and the pseudo-second-order kinetic models and thermodynamics. Dye–biosorbent interactions were examined by FTIR and SEM analysis. The dynamic flow biosorption performance of the biosorbent system was also investigated.

2. Materials and methods

2.1. Apparatus

A Unicam UV2-100 model UV/vis spectrophotometer equipped with a tungsten lamp was used to determine the dye concentrations in the solutions at λ_{max} of 586 nm. All pH measurements were performed with a WTW INOLAB 720 model digital pH meter. FTIR spectral analysis of unloaded and dye-loaded biosorbent was recorded in a PerkinElmer Spectrum 100IR infrared spectrometer in the region of 400–4000 cm^{-1} and the samples were prepared as KBr pellets under high pressure. The surface structure and morphology of the biosorbent material before and after dye biosorption were characterized using a scanning electron microscope (JEOL 560 LV SEM), at 20 kV and a 1000× magnification. Prior to analysis, the samples were coated with a thin layer of gold under an argon atmosphere to improve electron conductivity and image quality. The surface charge of the biomass was measured using a Zeta potential analyzer (Malvern Zetasizer nano ZS).

2.2. Preparation of mixed biosorbent

The macro-fungus *A. bisporus* was purchased from a commercial company and *T. orientalis* cones were naturally collected in July 2007. The samples were repeatedly washed with deionized water to remove adhering dirt and soluble impurities. They were then dried at 80 °C for 24 h and crushed and sieved to a particle size of under 150 μm using an ASTM standard sieve.

The *T. oriantalis* cones were used as a biomatrix and the procedure [19] recommended by Mahan and Holcombe was used to prepare the mixed biosorbent. The *A. bisporus*/*T. oriantalis* ratio used was 1:2, and a solid mixture of the biological samples was prepared. The powder mixture was wetted with 5 mL of deionized water and thoroughly mixed. The paste was heated in an oven at 80 °C for 24 h to dry the mixture. The wetting and drying steps were repeated to improve the biosorption efficiency. The mixed biosorbent was then crushed to obtain the original particle size. The powdered mixed biosorbent was stored in a glass bottle prior to biosorption studies.

2.3. RB49 solutions

The RB 49 dye was selected as a representative reactive dye for this study. Its chemical structure is shown in Fig. 1. A stock solution of RB49 was prepared by dissolving 1.0 g of RB49 in 1 L of deionized water, and the concentrations of RB49 used in this study (100–1000 mg L^{-1}) were obtained by dilution of the stock solution. The pH of the solution was adjusted to the desired value by adding a small quantity of 0.1 mol L^{-1} HCl or 0.1 mol L^{-1} NaOH.

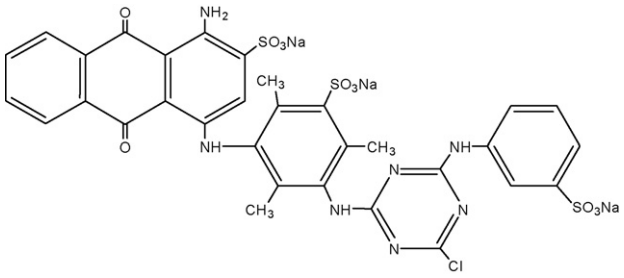

Fig. 1. Chemical structure of RB49.

2.4. Batch biosorption studies

Batch biosorption studies were conducted in 100 mL glass beakers. RB49 solutions were used at a concentration of 150 mg RB49 L^{-1}, with pH values ranging from 1 to 10. Fifty milliliters of the RB49 solution was added to each beaker with 0.05 g of mixed biosorbent. The mixture was stirred at 200 rpm for 60 min using a digitally controlled magnetic stirrer. The samples were centrifuged at 4500 rpm for 3 min to separate the solid phase from the liquid phase. The supernatants were analyzed to determine the concentration of the RB49 that remained by spectrophotometer. In order to determine the maximum biosorption yield, biosorbent samples at concentrations ranging between 0.2 and 4.0 g L^{-1} were mixed with RB49 solutions (at an initial pH of 1.0) and stirred for 60 min. After centrifugation, the samples were analyzed for RB49, as described above. The relationship between contact time, temperature and biosorption efficiency of the dye was determined using a batch test. The contact time between the dye and the biomass ranged from 5 to 90 min and the temperatures ranged from 25 to 45 °C. The pseudo-first-order and the pseudo-second-order kinetic models were applied to data. The Langmuir, Freundlich and D–R isotherm models were investigated in batch mode using an initial RB49 concentration range of 100–1000 mg L^{-1} and varying operating temperatures.

2.5. Column biosorption studies

The performance of the mixed biosorbent was investigated in a continuous mode using an up flow packed glass column. A known quantity of biomass was packed between two layers of glass wool into the column to provide the desired bed height. The RB49 solution was pumped from the bottom of the column to the top at a desired flow rate using a peristaltic pump (Ismatec ecoline). All of the column studies were performed at room temperature (25 ± 0.5 °C) and the temperature was periodically checked during the column process. In the first stage of the column biosorption studies, the flow rate of sorbate was altered in a range between 0.5 and 7.0 mL min^{-1}, while all of the other parameters, such as pH, amount of biosorbent, temperature, initial dye concentration, column i.d. and sorbate volume were kept constant. The effect of column i.d. on the biosorption performance was investigated by using different columns (9–19 mm i.d. and 100 mm height). The effluent samples left the column and were collected (in a 50 mL volume) and analyzed at λ_{max} of 586 nm as described above.

3. Results and discussion

The biosorption capacities of *A. bisporus* and *T. orientalis* were found as 69.51 and 14.93 mg g^{-1} for RB49. The mixed biosorbent has the biosorption capacity of 72.86 mg g^{-1} at same experimental conditions. In the case of a combination of these biosorbents, the biosorption capacity of *T. orientalis* increased by 4.88-fold while the

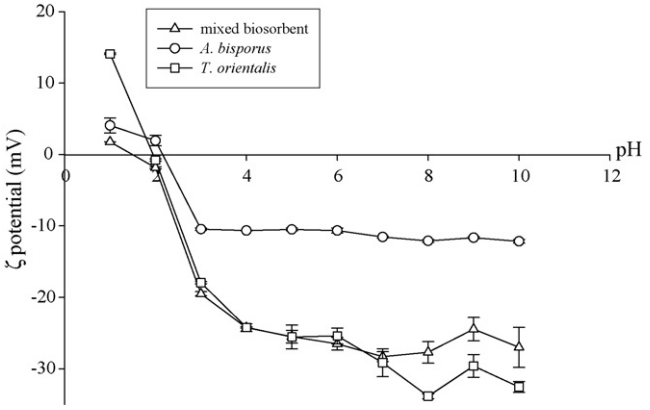

Fig. 2. Variation of zeta potentials of mixed biosorbent, *A. bisporus* and *T. orientalis* under different pH conditions.

biosorption capacity of *A. bisporus* slightly increased. Advantage of the use of mixed biosorbent is the low cost of the biosorption process. *T. orientalis* cones are widely available in large quantity. Hence, the almost the same amount of RB49 pollution could be removed with lower amount of *A. bisporus* in a mixture of raw materials.

3.1. The effect of initial pH on biosorption

Dye-bearing wastewaters generally differ in their pH values. The dye–biosorbent interaction depends on the structures of the dye and biosorbent. Dyes are complex aromatic organic compounds with unsaturated bonds and different functional groups. Therefore, they have different degrees of ionization at different pH values, and this alters the net charge on dye molecules. The net charge on the biosorbent is also pH-dependent because the biosorbent surface has biopolymers with many different functional groups. Therefore, the pH of the medium is an important environmental parameter for dye removal from the aqueous medium [13].

Since there was a close relationship between the zeta potential and the biosorption capacity of biomaterials [20], the changes in the surface charge of the biomass could be determined. Fig. 2 indicates the zeta potential of the biomass under different pH conditions. The point of zero charge of the biosorbent, pH_{pzc}, was around 1.5. The acidic value of pH_{pzc} could be due to the presence of anionic groups on the biosorbent surface that dominate over the cationic groups. The presence of polysaccharides, phosphates and amino groups on the cell wall give a net charge on the surface that depending on the pH [21]. When the pH of the solution increases, the number of positively charged available sites decreases, and the number of negatively charged sites increases. The surface of the biosorbent becomes negatively charged, and this decreases the biosorption of the negatively charged RB49 anions through electrostatic forces of repulsion. Therefore, the biosorption of reactive dye anions increases at lower pH values.

Fig. 3 shows the effect of initial pH on RB49 uptake using mixed biosorbent. As the pH of the aqueous medium increased from 1.0 to 4.0, the biosorption capacity of the biomass decreased from 72.86 to 7.72 mg g^{-1} and it remained nearly constant within the range of pH 4.0–10.0. The optimal initial pH for biosorption was 1.0 and these results were also consistent with the trend in zeta potential observed for the mixed biosorbent.

3.2. Effect of biosorbent dosage

The biosorption performance of the mixed biosorbent was tested by using different amounts of sorbent and these results are presented in Fig. 4.

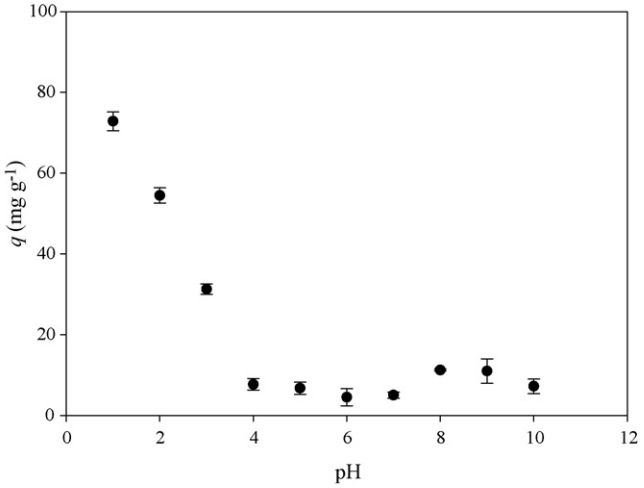

Fig. 3. Initial pH effect on the biosorption of RB49 using mixed biosorbent (m: 1.0 g L^{-1}; C_0: 150 mg L^{-1}; t: 60 min).

Fig. 4 shows that the percentage biosorption yield increased from 2.78 to 84.70% when the biomass concentration increased from 0.2 to 3.0 g L^{-1}. The increase in biosorption yield with biomass concentration may be attributed to the increased surface area of biomass and availability of possible biosorption sites [22]. Similar findings have also reported by other researchers [23,24]. A further increase in biomass concentration over 3.0 g L^{-1} did not lead to a significant improvement in biosorption yield due to saturation of the biosorbent surface with dye molecules [25]. Therefore, the optimal biomass concentration was selected as 3.0 g L^{-1} for the further experiments.

3.3. Time of equilibrium as a function of temperature

The time dependency of batch mode biosorption was tested at 25, 35 and 45 °C by varying the contact time between 10 and 90 min. Fig. 5 shows that for the given temperatures, the biosorption capacity of biomass increased in a linear manner with time and the biosorption equilibrium was established within 40 min. The equilibrium biosorption capacities of the mixed biosorbent were 41.35, 44.45 and 48.07 mg g^{-1} at temperatures of 25, 35 and 45 °C, respectively. After this period, dye biosorption was virtually constant. The

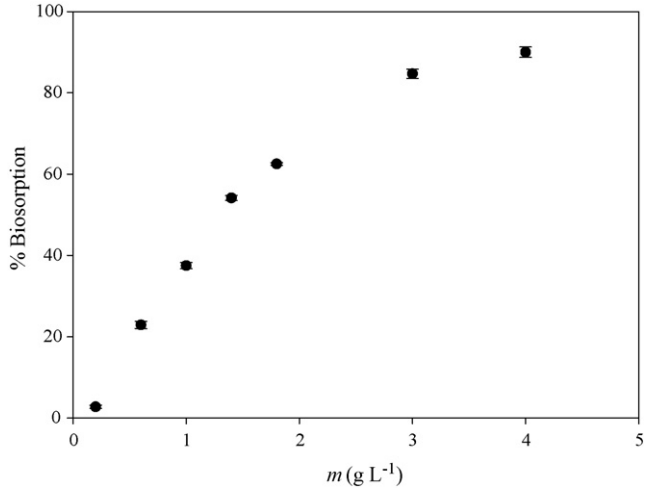

Fig. 4. Effect of biosorbent dosage on the biosorption of RB49 using mixed biosorbent (pH: 1.0; C_0: 150 mg L^{-1}; t: 60 min).

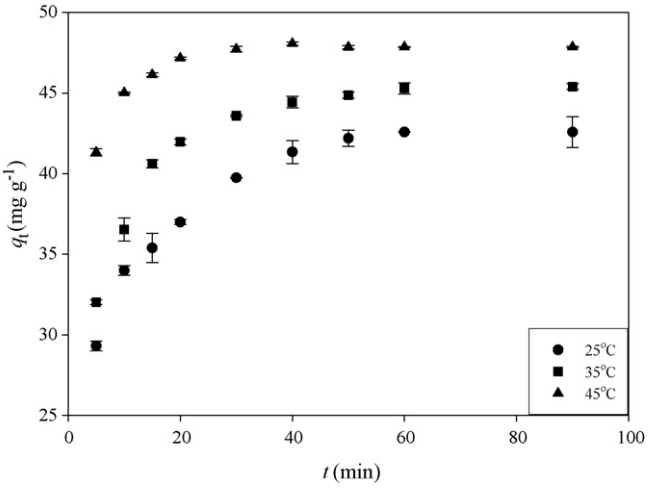

Fig. 5. Effect of contact time on the biosorption of RB49 using mixed biosorbent at different temperatures (pH: 1.0; C_0: 150 mg L^{-1}; m: 3.0 g L^{-1}).

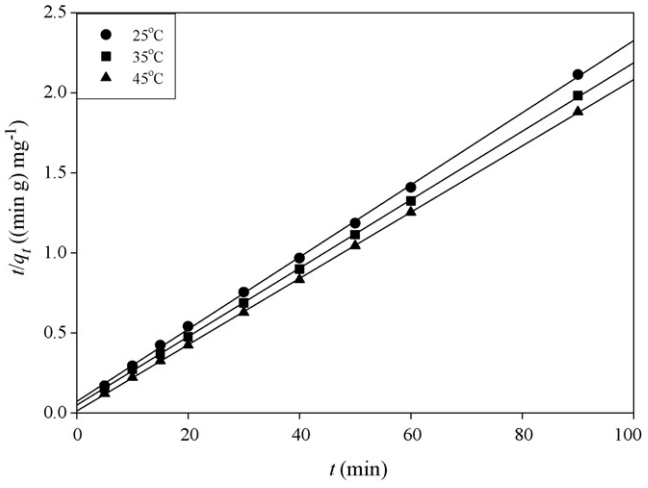

Fig. 6. Pseudo-second-order kinetic plots for the biosorption of RB49 by mixed biosorbent at different temperatures.

observed trend in increased biosorption capacity with increasing temperature suggests that biosorption of the RB49 dye by mixed biosorbent is kinetically controlled by an endothermic process.

The higher biosorption rate that was observed at the beginning of biosorption process may be explained by an increase in the number of sorbent binding sites, which would result in an increased concentration gradient between sorbate in the solution and on the biomass surface. Since the biosorption of RB49 dye molecules onto vacant binding sites was decreased with an increase in contact time, the concentration gradient was reduced [26].

3.4. Biosorption kinetics

The equilibrium of sorption and sorption kinetics are two important physicochemical factors to consider when evaluating a sorption process. Sorption kinetics can explain the dependency of sorption rates upon the concentrations of sorbate in solution, and how sorption rates are affected by sorption capacity, or by the character of the sorbent [27]. Since the principles underlying biosorption kinetics include fitting the model that represents the experimental data best [26], the pseudo-first-order and the pseudo-second-order kinetic models were tested in our study.

The Lagergren pseudo-first-order rate expression [28] is given by the following equation:

$$\ln(q_e - q_t) = \ln q_e - K_L t \quad (1)$$

where q_e and q_t are the dye biosorbed at equilibrium and time t (mg g^{-1}), respectively. K_L is the rate constant for pseudo-first-order biosorption (min^{-1}). A straight line of $\ln(q_e - q_t)$ versus t (figure not shown) would suggest that this kinetic model is applicable to the data tested, and K_L and q_e were determined from the slope and intercept of the plot, respectively. The kinetic data in Table 1 demonstrate that the biosorption of RB49 onto mixed biosorbent does not follow pseudo-first-order kinetics.

The pseudo-second-order rate equation [29] is given by

$$\frac{t}{q_t} = \frac{1}{k_2 q_2^2} + \frac{1}{q_2} t \quad (2)$$

where k_2 is the pseudo-second-order rate constant (g mg^{-1} min^{-1}) and q_2 is the equilibrium biosorption capacity (mg g^{-1}). Values of k_2 and q_2 were calculated from a plot of t/q_t against t (Fig. 6).

As seen in Table 1, the r^2 values for the pseudo-first-order and the pseudo-second-order kinetic models indicated that the pseudo-first-order kinetic model could not explain the biosorption kinetics in our study. However, the calculated equilibrium biosorption capacities from the pseudo-second-order kinetic model with r^2 values of 0.999 showed good agreement with the experimental values at all temperatures studied. The higher linear r^2 values confirm that the biosorption data are well represented by the pseudo-second-order model for the entire biosorption period and thus support the assumption behind the model that the biosorption is due to chemisorption. The pseudo-second-order rate constants for the biosorption of RB49 dye onto biosorbent show a steady increase with temperature. The values of rate constants were found to increase from 7.09×10^{-3} to 3.54×10^{-2} g mg^{-1} min^{-1} with an increase in the solution temperatures from 25 to 45 °C, indicating that the biosorption of RB49 dye onto mixed biosorbent is rate-controlled (Table 1).

3.5. Column biosorption studies

Although the results from the batch biosorption study provided fundamental information regarding the biosorbent behavior and dye biosorption performance [26], a continuous mode of operation is preferred for large-scale water treatment applications. A continuously operating system has advantages such as simple operation, high yield, is easily scaled up from the laboratory and the packed bed of biosorbent is easy to regenerate [4]. Therefore, the mixed biomass system developed in this study was also used to evaluate RB49 biosorption in a continuous mode.

Table 1
Kinetic parameters for the biosorption of RB49 onto mixed biosorbent at various temperatures

t (°C)	K_L (min^{-1})	q_e (mg g^{-1})	r_1^2	k_2 (g mg^{-1} min^{-1})	q_2 (mg g^{-1})	r_2^2
25	3.11×10^{-2}	7.53	0.714	7.09×10^{-3}	44.37	0.999
35	2.81×10^{-2}	5.70	0.576	9.25×10^{-3}	46.79	0.999
45	3.91×10^{-2}	3.17	0.708	3.54×10^{-2}	48.32	0.999

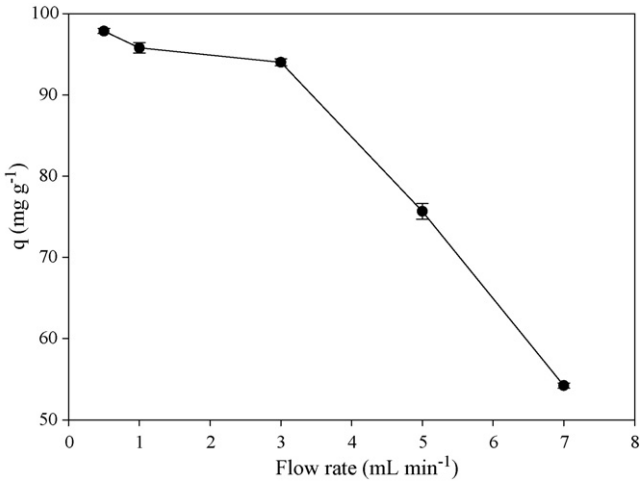

Fig. 7. Effect of flow rate on the biosorption of RB49 by mixed biosorbent (pH: 1.0; C_0: 150 mg L^{-1}; m: 3.0 g L^{-1}; column i.d.: 9.0 mm).

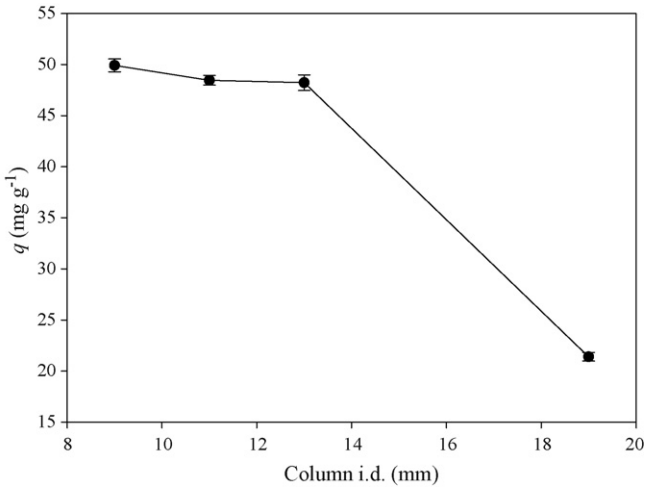

Fig. 8. Effect of column size on the biosorption of RB49 by mixed biosorbent (pH: 1.0; C_0: 150 mg L^{-1}; m: 3.0 g L^{-1}; flow rate: 0.5 mL min^{-1}).

The flow rate of sorbate was varied from 0.5 to 7 mL min^{-1} to evaluate the effect of flow rate on the biosorption capacity of mixed biosorbent. These results are shown in Fig. 7. The flow rate strongly influenced RB49 uptake capacity, and lower flow rates favor RB49 biosorption. The biosorption capacity of the mixed biosorbent significantly decreased with increased flow rate [30]. At lower flow rates, RB49 had more time in contact with the biosorbent, resulting in more RB49 being removed from the column. High flow rates reduce the contact time between the dye molecules and biosorbent by reducing the solute residence time [31]. Therefore, the RB49 biosorption capacity of the mixed biosorbent was reduced from 97.84 to 54.22 mg g^{-1} with an increase in the flow rate from 0.5 to 7.0 mL min^{-1}. The optimal flow rate for RB49 biosorption was chosen as 0.5 mL min^{-1} in this study.

In order to investigate the effect of column size on biosorption performance, the column i.d. was changed from 9 to 19 mm and the results of these experiments are shown in Fig. 8.

The RB49 biosorption capacity of biosorbent was increased from 21.40 to 49.92 mg g^{-1} when the column i.d. was decreased from 19 to 9 mm. As the column i.d. was increased, the bed height was decreased because the amount of loading biomass into column was kept constant. Therefore, the maximum biosorption capacity was observed when a column with the lowest ID was used.

3.6. Biosorption isotherms

The isotherm models are widely used parameters to describe the equilibrium between biosorption capacity (q_e) and sorbate concentration (C_e) at a constant temperature. In this study, the equilibrium data were experimentally determined and three different models, the Langmuir, Freundlich and D–R were fitted to the data. The model constants calculated are presented in Table 2.

The Langmuir parameters can be derived from a linearized form of Eq. (3) [32] represented by

$$\frac{1}{q_e} = \frac{1}{q_{max}} + \left(\frac{1}{q_{max}K_L}\right)\ \frac{1}{C_e} \tag{3}$$

where q_e and q_{max} are the equilibrium and monolayer biosorption capacities of the sorbent (mol g^{-1}), respectively, C_e is the equilibrium RB49 concentration in the solution (mol L^{-1}) and K_L is the biosorption equilibrium constant (L mol^{-1}) related to the free energy of biosorption. q_{max} indicates a practical limiting biosorption capacity when all binding sites are occupied by dye molecules, and allows comparison of biosorption performances [25]. The Langmuir isotherm plots at different temperatures are shown in Fig. 9. The r^2 and q_{max} values in Table 2 suggested that the Langmuir isotherm might be a suitable model for out data due to the high correlation coefficients. It was concluded that the biosorption process of RB49 by mixed biosorbent was monolayer biosorption, and the maximum monolayer biosorption capacities were found between 1.34×10^{-4} mol g^{-1} (118.26 mg g^{-1}) and 1.85×10^{-4} mol g^{-1} (153.26 mg g^{-1}) at the various temperatures used in this study.

The Langmuir constant, K_L, can be used to determine the suitability of the biosorbent for the sorbate using the Hall separation factor (R_L) as follows [33,34]:

$$R_L = \frac{1}{1 + K_L C_0} \tag{4}$$

where C_0 is the highest initial sorbate concentration (mol L^{-1}). R_L is the constant separation factor (dimensionless) and can be used

Table 2
Biosorption isotherm constants for the biosorption of RB49 onto mixed biosorbent at various temperatures

	q_{exp} (mol g^{-1})	Langmuir				Freundlich			Dubinin–Radushkevich (D–R)			
		q_{max} (mol g^{-1})	K_L (L mol^{-1})	r^2_L	R_L	n	K_F (L g^{-1})	r^2_F	q_{max} (mol g^{-1})	β (mol^2 kJ^{-2})	r^2_{D-R}	E (kJ mol^{-1})
Batch (25 °C)	1.68×10^{-4}	1.34×10^{-4}	6.44×10^{5}	0.985	1.25×10^{-2}	3.596	1.33×10^{-3}	0.958	3.61×10^{-4}	1.53×10^{-3}	0.976	14.58
Batch (35 °C)	1.92×10^{-4}	1.64×10^{-4}	4.38×10^{5}	0.990	1.83×10^{-2}	2.958	2.67×10^{-3}	0.951	5.43×10^{-4}	1.64×10^{-3}	0.972	13.67
Batch (45 °C)	2.06×10^{-4}	1.85×10^{-4}	3.93×10^{5}	0.994	2.03×10^{-2}	2.817	3.41×10^{-3}	0.934	6.40×10^{-4}	1.62×10^{-3}	0.960	13.79
Column	1.39×10^{-4}	1.32×10^{-4}	6.77×10^{5}	0.986	1.69×10^{-2}	3.448	1.52×10^{-3}	0.940	3.82×10^{-4}	1.56×10^{-3}	0.963	14.37

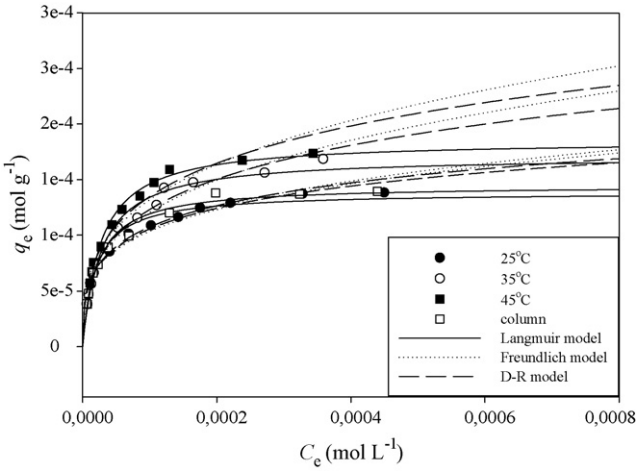

Fig. 9. Biosorption isotherm plots for the biosorption of RB49 by mixed biosorbent at in batch and continuous systems (pH: 1.0; m: 3.0 g L^{-1}).

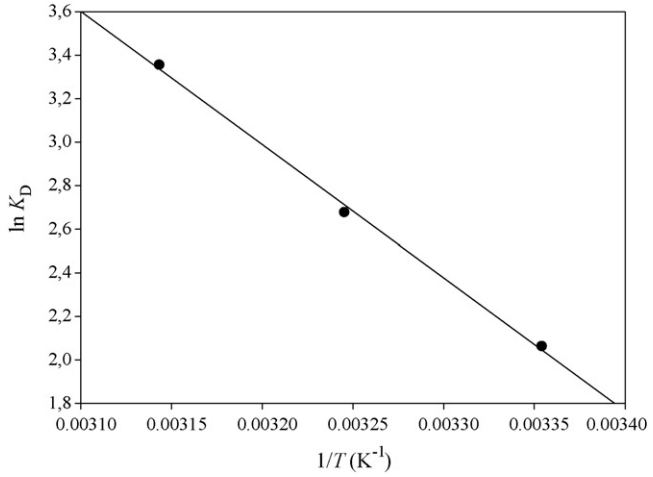

Fig. 10. Plot of ln K_D versus 1/T for estimation of thermodynamic parameters.

for interpretation of the sorption type as follows [35]:

$R_L > 1$, unfavorable
$R_L < 0$, unfavorable
$R_L = 1$, favorable (linear)
$0 < R_L < 1$, favorable
$R_L = 0$, irreversible

In this study, we found values of R_L between 1.25×10^{-2} and 2.03×10^{-2}, and this, along with the shape of the curve of the data (Fig. 9) indicates that the biosorption [36] of RB49 by mixed biosorbent is favorable.

Biosorption–partition constants were determined for RB49 using the following linearized Freundlich equation:

$$\ln q_e = \ln K_F + \frac{1}{n} \ln C_e \quad (5)$$

where K_F (L g^{-1}) is the Freundlich constant, which indicates biosorbent capacity and n (dimensionless) is the Freundlich exponent, which is related to biosorbent intensity [37].

The Freundlich isotherm plots for RB49 biosorption by the mixed biosorbent at different temperatures are shown in Fig. 9. The values of K_F and n at the different temperatures ranged between 1.33×10^{-3} to 3.41×10^{-3} and 3.596–2.817, respectively (Table 2).

Since the Freundlich and Langmuir isotherm models do not provide any insights into the biosorption mechanism, the equilibrium data were tested with the D–R isotherm model. The D–R model was used to estimate the mean free energy of biosorption. The following equation indicates the linearized D–R isotherm [38]:

$$\ln q_e = \ln q_m - \beta\varepsilon^2 \quad (6)$$

where $\varepsilon = RT\ln(1 + 1/C_e)$ (Polanyi potential), q_m is the biosorption capacity (mol g^{-1}), β is the constant related to the biosorption energy, R is the gas constant and T is the temperature (K). The D–R plots for RB49 biosorption are shown in Fig. 9.

The Polanyi sorption theory assumes [39] that there is a fixed volume of sorption space close to the sorbent surface, and that sorption potential exists over these spaces. The mean free energy of biosorption (E) can be calculated from the equation:

$$E = \frac{1}{(2\beta)^{1/2}} \quad (7)$$

The magnitude of E is useful for estimating the type of biosorption process, and the value of E was found to range between 14.58 and 13.67 kJ mol^{-1} in this study. These values are within the energy range of sorption reactions (8–16 kJ mol^{-1}). If the interval of (8–16 kJ mol^{-1}) is taken into consideration [40], RB49 biosorption by mixed biosorbent may be classified as chemical sorption.

The isotherm equations shown above were also applied to continuous biosorption data and similar results were obtained as with batch conditions, 1.34×10^{-4} mol g^{-1} at 25 °C (room temperature) (Table 2). The maximum monolayer capacity was 1.32×10^{-4} mol g^{-1} under column conditions. These results were also consistent with an experimental q_{max} value of 1.39×10^{-4} mol g^{-1}.

3.7. Thermodynamic analysis of biosorption

Thermodynamic parameters (energy and entropy) are used to determine whether a biosorption process will spontaneously occur. RB49 biosorption may be represented by the following reversible process [41]:

dye in solution ⇌ dye-mixed biosorbent

For such equilibrium reactions, K_D, the distribution constant, can be used to calculate the Gibbs free energy:

$$K_D = \frac{q_e}{C_e} \quad (8)$$

$$\Delta G^\circ = -RT \ln K_D \quad (9)$$

$$\ln K_D = -\frac{\Delta G^\circ}{RT} = -\frac{\Delta H^\circ}{RT} + \frac{\Delta S^\circ}{R} \quad (10)$$

where R is the universal gas constant, 8.314 J mol^{-1} K^{-1}, and T is the absolute temperature in K. The ΔS° and ΔH° values were calculated from the slope and intercept of a Van't Hoff plot (Fig. 10) of ln K_D versus 1/T, respectively. The negative values of ΔG° at different temperatures (Table 3) indicate that RB49 biosorption is a spontaneous process and the mixed biosorbent has higher affinity at higher temperatures. A decrease in the magnitude of ΔG° values with an increase in the temperature may be attributed to a reduction in the spontaneity degree at studied temperatures [42].

Table 3
Thermodynamic parameters calculated from the pseudo-second-order kinetic model for the biosorption of RB49 onto mixed biosorbent

t (°C)	K_D	ΔG° (kJ mol^{-1})	ΔH° (kJ mol^{-1})	ΔS° (J K^{-1} mol^{-1})
25	7.88	−5.06		
35	14.56	−6.94	50.93	187.80
45	28.69	−8.82		

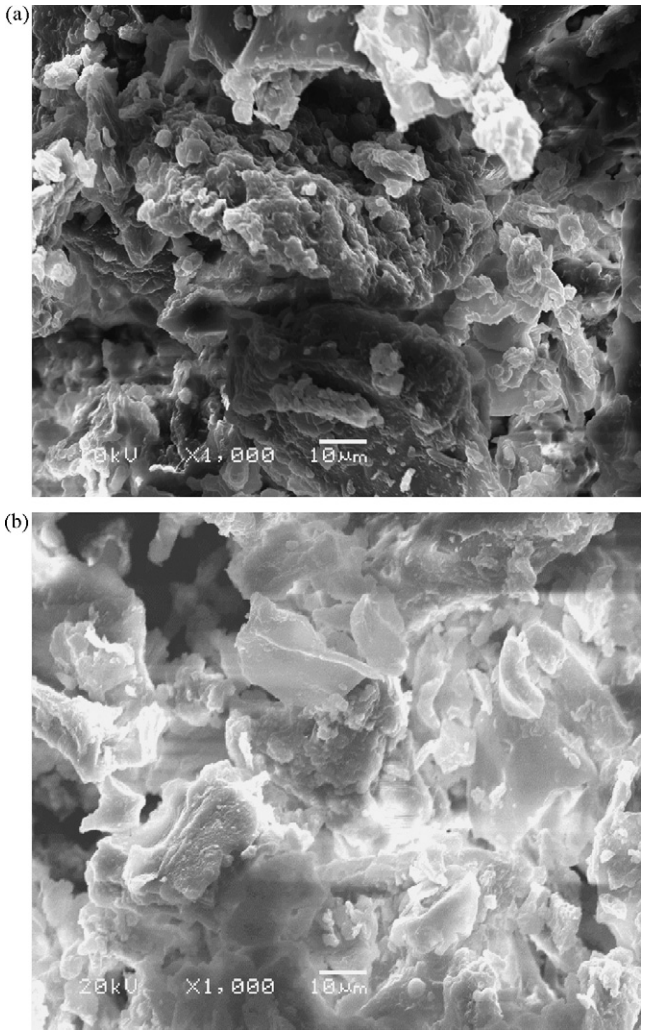

Fig. 11. SEM micrographs for (a) mixed biosorbent and (b) RB49-loaded-mixed biosorbent.

The change in the standard enthalpy, ΔH° is 50.93 kJ mol^{-1}. The positive ΔH° value shows that biosorption of RB49 dye by mixed biosorbent is an endothermic process and reflects the affinity of mixed biosorbent for RB49. This trend may be explained by availability of more active sites of adsorbent at higher temperatures due to increased surface activity and increased kinetic energy of the RB49 molecules.

The positive ΔS° value (+187.80 J K^{-1} mol^{1}) indicates that randomness at the solid–solute interface increases with RB49 biosorption onto the biosorbent [43], suggests good affinity of RB49 towards the biosorbent and reflects some structural changes in sorbate and biosorbent. The similar findings were also reported in the literature [26,44–46].

3.8. Characterization of the biosorbent and biosorption mechanism

The biosorbent used in this study was analyzed by scanning electron microscopy to examine its textural structure. An SEM micrograph of unloaded biomass is shown in Fig. 11(a), and indicates the fibrous structure of the biomass. The biosorbent has irregular pores with a diameter of about 10 μm, which indicates that the mixed biosorbent has a porous structure [47]. This structural feature of the biomass may be important since it increases

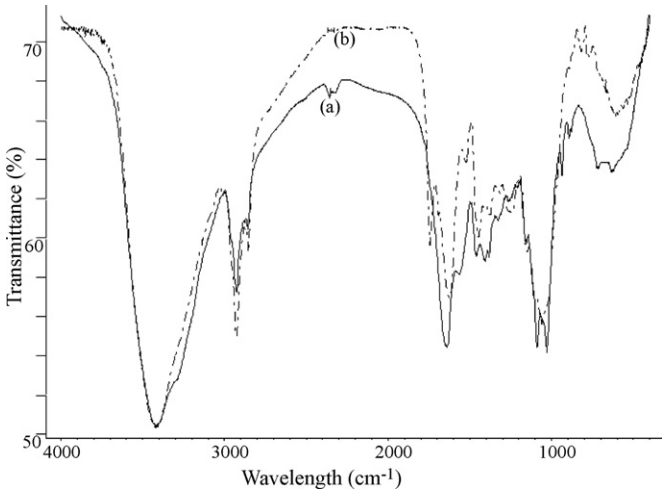

Fig. 12. FTIR spectra for *A. bisporus* (a) and *T. orientalis* (b).

the total surface area [48]. Fig. 11(b) shows an SEM micrograph of the biomass loaded with dye. The biomass structure changed upon sorbing the RB49, and had a tendency to form agglomerates [49]. There was also an observed decrease in pore sizes in the biomass, and this may be attributed to the fact that the porous structure plays a role in RB49 biosorption.

The FTIR spectra of *A. bisporus* and *T. orientalis* were given in Fig. 12 in order to characterize the raw materials of mixed biosorbent. The similar functional groups were observed in the FTIR spectra of both raw materials. The FTIR spectra of unloaded and dye-loaded mixed biosorbent in a range of 400–4000 cm^{-1} were analyzed in order to discover which functional groups are responsible for the biosorption process. These data are presented in Fig. 13. The unloaded biomass has a very complex structure and has a number of absorption peaks. It has previously been reported that all of the biological sorbent materials have intense absorption bands around 3500–3200, which represent the stretching vibrations of amino groups. These bands are superimposed onto the side of the hydroxyl group band at 3500–3300 cm^{-1} [48]. A similar and very strong absorption peak was observed for both unloaded and dye-loaded biomass at about 3400 cm^{-1}. The spectra of the unloaded and RB49-loaded biomass also display absorption peaks at 3011, 2926 and 2854 cm^{-1}, corresponding to stretching of the C—H bonds of the methyl and methylene groups present in the lignin structure

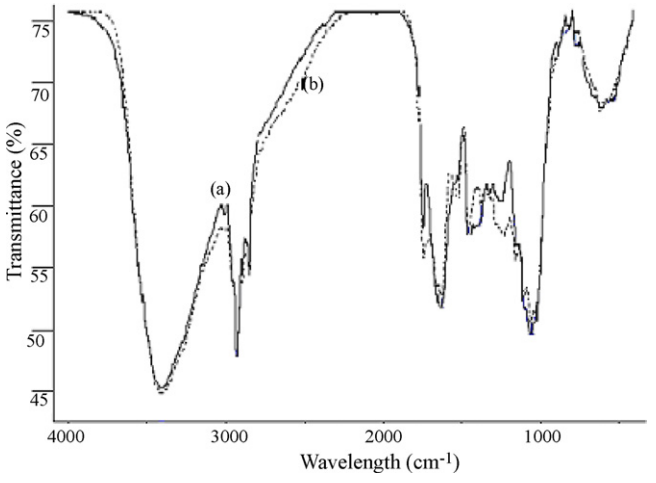

Fig. 13. FTIR spectra for (a) mixed biosorbent and (b) RB49-loaded-mixed biosorbent.

[50]. The carboxyl groups showed a characteristic absorption peak at 1744 cm^{-1} for unloaded biomass, and this band slightly shifted to a lower frequency (1740 cm^{-1}) after RB49 biosorption. —C=O chelate stretching of the amid-I band was observed at 1627 cm^{-1} for both unloaded and dye-loaded biomass. The appearance of an amid-II band at 1526 cm^{-1} and —C—N stretching vibrations at 1159 and 1106 cm^{-1} [51] for dye-loaded biomass may be attributed to biosorption of RB49 molecules onto the biomass surface. The —OH bending vibrations at 1412 cm^{-1} and bands at 1261 cm^{-1} that corresponded to bending vibrations of the O—C—H, C—C—H and C—O—H groups [50] in the unloaded biomass disappeared in the FTIR spectrum of the dye-loaded biomass. The absorption peaks around 1163 and 1078 cm^{-1} are indicative of P=O stretching and P—OH stretching vibrations, respectively [52]. The band between 611 and 520 cm^{-1} for the mixed biosorbent represents C—N—C scissoring that is only found in protein structures [48], and this band disappeared after RB49 biosorption.

The FTIR spectrum of the unloaded biomass indicates that amine groups are present, and these are likely to be responsible for RB49 binding. The spectra also indicate that carboxyl and phosphonate groups are also present in the biomass, and these groups may electrostatically inhibit RB49 binding at the higher pH value of 3.0 [53]. The alterations observed in the FTIR spectra upon dye loading indicated the groups that were potentially involved in the biosorption process on the biomass surface.

4. Conclusions

A biosorbent mixture of *A. bisporus* and *T. orientalis* was found to be an effective biosorbent for the removal of a reactive dye (RB49) from contaminated solutions in both batch and continuous biosorption processes. Batch studies demonstrated that the kinetics were well described by the pseudo-second-order model, and the equilibrium was well described by the Langmuir model in the temperature ranges studied. The temperature dependence data indicated that the biosorption process was spontaneous and endothermic. Dynamic flow studies revealed the importance of flow rate, column size and inlet solute concentration in the biosorption process. The dye–biosorbent interactions were confirmed by FTIR and SEM analysis and the functional groups such as carboxyl, amine, amide and hydroxyl on the biosorbent surface were found as responsible for RB49 biosorption. In conclusion, the biomass system proposed in this study may be an economic, effective and eco-friendly option for the removal of reactive dyes from aqueous media.

References

[1] P.C. Vandevivere, R. Bianchi, W. Verstraete, Treatment and reuse of wastewater from the textile wet-processing industry: review of emerging technologies, J. Chem. Technol. Biotechnol. 72 (1998) 289–302.

[2] E.Y. Ozmen, S. Erdemir, M. Yilmaz, M. Bahadir, Removal of carcinogenic direct azo dyes from aqueous solutions using calix[*n*]arene derivatives, Clean 35 (2007) 612–616.

[3] O.J. Hao, H. Kim, P.C. Chiang, Decolorization of wastewater, Crit. Rev. Environ. Sci. Technol. 30 (2000) 449–505.

[4] Z. Aksu, Ş. Şen Çağatay, F. Gonen, Continuous fixed bed biosorption of reactive dyes by dried *Rhizopus arrhizus*: determination of column capacity, J. Hazard. Mater. 143 (2007) 362–371.

[5] H. Lata, V.K. Garg, R.K. Gupta, Removal of a basic dye from aqueous solution by adsorption using *Parthenium hysterophorus*: an agricultural waste, Dyes Pigments 74 (2007) 653–658.

[6] E. Rubin, P. Rodriguez, R. Herrero, J. Cremades, I. Barbara, M.E. Sastre de Vicente, Removal of Methylene Blue from aqueous solutions using as biosorbent *Sargassum muticum*: an invasive macroalga in Europe, J. Chem. Technol. Biotechnol. 80 (2005) 291–298.

[7] Y. Fu, T. Viraraghavan, Dye biosorption sites of *Aspergillus niger*, Bioresour. Technol. 82 (2002) 139–145.

[8] Z. Aksu, S. Tezer, Biosorption of reactive dyes on the green alga *Chlorella vulgaris*, Process Biochem. 40 (2005) 1347–1361.

[9] R. Aravindhan, J.R. Rao, B.U. Nair, Removal of basic yellow dye from aqueous solution by sorption on green alga *Caulerpa scalpelliformis*, J. Hazard. Mater. 142 (2007) 68–76.

[10] S. Tunali, A. Ozcan, Z. Kaynak, A.S. Ozcan, T. Akar, Utilization of the *Phaseolus vulgaris* L. Waste biomass for decolorization of the textile dye Acid Red 57: determination of equilibrium, kinetic and thermodynamic parameters, J. Environ. Sci. Health A 42 (2007) 591–600.

[11] G. Bayramoglu, M.Y. Arica, Biosorption of benzidine based textile dyes "Direct Blue 1 and Direct Red 128" using native and heat-treated biomass of *Trametes versicolor*, J. Hazard. Mater. 143 (2007) 135–143.

[12] N.S. Maurya, A.K. Mittal, P. Cornel, E. Rother, Biosorption of dyes using dead macro fungi: effect of dye structure, ionic strength and pH, Bioresour. Technol. 97 (2006) 512–521.

[13] J.T. Matheickal, Q. Yu, Biosorption of lead (II) from aqueous solutions by *Phellinus badius*, Miner. Eng. 10 (1997) 947–957.

[14] J. Vetter, Chitin content of cultivated mushrooms *Agaricus bisporus*, *Pleurotus ostreatus* and *Lentinula edodes*, Food Chem. 102 (2007) 6–9.

[15] E. Oguz, Adsorption characteristics and the kinetics of the Cr(VI) on the *Thuja oriantalis*, Colloid Surf. A 252 (2004) 121–128.

[16] Y. Nuhoglu, E. Oguz, Removal of copper(II) from aqueous solutions by biosorption on the cone biomass of *Thuja orientalis*, Process Biochem. 38 (2003) 1627–1631.

[17] E. Malkoc, Ni(II) removal from aqueous solutions using cone biomass of *Thuja orientalis*, J. Hazard. Mater. 137 (2006) 899–908.

[18] T. Akar, A.S. Ozcan, S. Tunali, A. Ozcan, Biosorption of a textile dye (Acid Blue 40) by cone biomass of *Thuja orientalis*: estimation of equilibrium, thermodynamic and kinetic parameters, Bioresour. Technol. 99 (2008) 3057–3065.

[19] C.A. Mahan, J.A. Holcombe, Immobilisation of algae cells on silica gel and their characterization for trace metal preconcentration, Anal. Chem. 64 (1992) 1933–1939.

[20] M. Dundar, C. Nuhoğlu, Y. Nuhoğlu, Biosorption of Cu(II) ions onto the litter of natural trembling poplar forest, J. Hazard. Mater. 151 (2008) 86–95.

[21] A.E.C. Botero, M.L. Torem, L.M.S. de Mesquita, Surface chemistry fundamentals of biosorption of *Rhodococcus opacus* and its effect in calcite and magnesite flotation, Miner. Eng. 21 (2008) 83–92.

[22] R. Gong, Y. Ding, M. Li, C. Yang, H. Liu, Y. Sun, Utilization of powdered peanut hull as biosorbent for removal of anionic dyes from aqueous solution, Dyes Pigments 64 (2005) 187–192.

[23] P. Waranusantigul, P. Pokethitiyook, M. Kruatrachue, E.S. Upatham, Kinetics of basic dye (methylene blue) biosorption by giant duckweed (*Spirodela polyrrhiza*), Environ. Pollut. 125 (2003) 385–392.

[24] A. Özer, G. Akaya, M. Turabik, The removal of Acid Red 274 from wastewater: combined biosorption and biocoagulation with *Spirogyra rhizopus*, Dyes Pigments 71 (2006) 83–89.

[25] G. Akkaya, A. Özer, Biosorption of Acid Red 274 (AR 274) on *Dicranella varia*: determination of equilibrium and kinetic model parameters, Process Biochem. 40 (2005) 3559–3568.

[26] K. Vijayaraghavan, Y.S. Yun, Biosorption of C.I. Reactive Black 5 from aqueous solution using acid-treated biomass of brown seaweed *Laminaria* sp., Dyes Pigments 76 (2008) 726–732.

[27] Y.S. Ho, J.C.Y. Ng, G. McKay, Kinetics of pollutant sorption by biosorbents: review, Sep. Purif. Method 29 (2000) 189–232.

[28] S. Lagergren, Zur theorie der sogenannten adsorption gelöster stoffe. Kungliga Svenska Vetenskapsakademiens, Handlingar 24 (1898) 1–39.

[29] Y.S. Ho, G. McKay, Kinetic models for the sorption of dye from aqueous solution by wood, Process Saf. Environ. 76 (B2) (1998) 183–191.

[30] R. Han, D. Ding, Y. Xu, W. Zou, Y. Wang, Y. Li, L. Zou, Use of rice husk for the adsorption of congo red from aqueous solution in column mode, Bioresour. Technol. 99 (2008) 2938–2946.

[31] M.G.A. Vieira, R.M. Oisiovici, M.L. Gimenes, M.G.C. Silva, Biosorption of chromium(VI) using a *Sargassum* sp. packed-bed column, Bioresour. Technol. 99 (2008) 3094–3099.

[32] I. Langmuir, The adsorption of gases on plane surfaces of glass, mica and platinum, J. Am. Chem. Soc. 40 (1918) 1361–1403.

[33] R. Nadeem, M.A. Hanif, F. Shaheen, S. Perveen, M.N. Zafar, T. Iqbal, Physical and chemical modification of distillery sludge for Pb(II) biosorption, J. Hazard. Mater. 150 (2008) 335–342.

[34] K.R. Hall, L.C. Eagleton, A. Acrivos, T. Vermeulen, Pore-and solid diffusion kinetics in fixed-bed adsorption under constant-pattern conditions, Ind. Eng. Chem. Fundam. 5 (1966) 212–223.

[35] S. Dahiya, R.M. Tripathi, A.G. Hegde, Biosorption of heavy metals and radionuclide from aqueous solutions by pre-treated arca shell biomass, J. Hazard. Mater. 150 (2008) 376–386.

[36] B. Kiran, A. Kaushik, Chromium binding capacity of *Lyngbya putealis* exopolysaccharides, Biochem. Eng. J. 38 (2008) 47–54.

[37] H.M.F. Freundlich, Über die adsorption in lösungen, Zeitschrift für Physikalische Chemie 57 (1906) 385–470.

[38] M.M. Dubinin, L.V. Radushkevich, Proc. Acad. Sci. U.S.S.R. Phys. Chem. Sect. 55 (1947) 331–333.

[39] J. Li, C.J. Werth, Modeling sorption isotherms of volatile organic chemical mixtures in model and natural solids, Environ. Toxicol. Chem. 21 (2002) 1377–1383.

[40] E. Oguz, Equilibrium isotherms and kinetics studies for the sorption of fluoride on light weight concrete materials, Colloid Surf. A 295 (2007) 258–263.

[41] V. Padmavathy, Biosorption of nickel(II) ions by baker's yeast: kinetic, thermodynamic and desorption studies, Bioresour. Technol. 99 (2008) 3100–3109.

[42] X.F. Sun, S.G. Wang, X.W. Liu, W.X. Gong, N. Bao, B.Y. Gao, H.Y. Zhang, Biosorption of Malachite Green from aqueous solutions onto aerobic granules: kinetic and equilibrium studies, Bioresour. Technol. 99 (2008) 3475–3483.
[43] N. Tewari, P. Vasudevan, B.K. Guha, Study on biosorption of Cr(VI) by *Mucor hiemalis*, Biochem. Eng. J. 23 (2005) 185–192.
[44] Z. Aksu, G. Karabayır, Comparison of biosorption properties of different kinds of fungi for the removal of Gryfalan Black RL metal-complex dye, Bioresour. Technol. 99 (2008) 7730–7741.
[45] R. Patel, S. Suresh, Kinetic and equilibrium studies on the biosorption of reactive black 5 dye by *Aspergillus foetidus*, Bioresour. Technol. 99 (2008) 51–58.
[46] Z. Aksu, A.İ. Tatlı, Ö. Tunç, A comparative adsorption/biosorption study of Acid Blue 161: effect of temperature on equilibrium and kinetic parameters, Chem. Eng. J. 142 (2008) 23–39.
[47] E.C. Lima, B. Royer, J.C.P. Vaghetti, N.M. Simon, B.M. da Cunha, F.A. Pavan, V. Benvenutti, R. Cataluna-Veses, C. Airoldi, Application of Brazilian pine-fruit shell as a biosorbent to removal of reactive red 194 textile dye from aqueous solution kinetics and equilibrium study, J. Hazard. Mater. 155 (2008) 536–550.
[48] G. Bayramoğlu, G. Çelik, M.Y. Arica, Biosorption of Reactive Blue 4 dye by native and treated fungus *Phanerocheate chrysosporium*: batch and continuous flow system studies, J. Hazard. Mater. 137 (2006) 1689–1697.
[49] W.T. Tsai, H.C. Hsu, T.Y. Su, K.Y. Lin, C.M. Lin, Removal of basic dye (methylene blue) from wastewaters utilizing beer brewery waste, J. Hazard. Mater. 154 (2008) 73–78.
[50] F.A. Pavan, E.C. Lima, S.L.P. Dias, A.C. Mazzocato, Methylene blue biosorption from aqueous solutions by yellow passion fruit waste, J. Hazard. Mater. 150 (2008) 703–712.
[51] D. Park, Y.S. Yun, J.M. Park, Studies on hexavalent chromium biosorption by chemically-treated biomass of *Ecklonia* sp., Chemosphere 60 (2005) 1356–1364.
[52] M.H. Han, Y.S. Yun, Mechanistic understanding and performance enhancement of biosorption of reactive dyestuffs by the waste biomass generated from amino acid fermentation process, Biochem. Eng. J. 36 (2007) 2–7.
[53] S.W. Won, S.B. Choi, B.W. Chung, D. Park, J.M. Park, Y.S. Yun, Biosorptive decolorization of Reactive Orange 16 using the waste biomass of *Corynebacterium glutamicum*, Ind. Eng. Chem. Res. 43 (2004) 7865–7869.